Microelectronic Engineering 178 (2017) 26–29

Contents lists available at ScienceDirect

Microelectronic Engineering

journal homepage: www.elsevier.com/locate/mee

A physically based model for resistive memories including a detailed temperature and variability description

G. González-Cordero [a], M.B. González [b], H. García [c], F. Campabadal [b], S. Dueñas [c], H. Castán [c], F. Jiménez-Molinos [a], J.B. Roldán [a,*]

[a] Departamento de Electrónica y Tecnología de Computadores, Universidad de Granada, 18071 Granada, Spain
[b] Institut de Microelectrònica de Barcelona, IMB-CNM (CSIC), Campus UAB, 08193 Bellaterra, Spain
[c] Departamento de Electrónica, Universidad de Valladolid, Paseo de Belén 15, 47011 Valladolid, Spain

ARTICLE INFO

Article history:
Received 17 February 2017
Received in revised form 18 April 2017
Accepted 19 April 2017
Available online 25 April 2017

Keywords:
Resistive RAM
ReRAM
Physical model
Stochastic variability

ABSTRACT

A new model to account for variability in resistive memories is presented. It is included in a previous general current model that considers the main physical mechanisms involved in the conductive filament formation and disruption processes that lead to different resistive states. The validity of the model has been proved for different technologies of metal-insulator-metal bipolar resistive memories. The model can be implemented in Verilog-A for circuit simulation purposes.

1. Introduction

Resistive Random Access Memories (RRAMs) are known to be one of the most promising alternatives to substitute flash technology in the non-volatile memory market [1,2]. In addition to fabrication developments, simulation and compact modeling are essential facets to make a new technology pass into the maturity state. In this context, the variability of resistive switching (RS) based on the formation and disruption of Conductive Filaments (CF) in Metal-Insulator-Metal (MIM) structures has been modeled in this manuscript. The model works well for MIM structures fabricated with different technologies, once the corresponding model parameters are fitted. The resistance of the electrodes and that of the CFs in different stages of formation is considered, as well as the hopping current in the gap (g) between the CF tip and the electrode. The thermal description of the CF is included by solving the heat equation where Joule heating and lateral dissipation from the CF to the surrounding dielectric are taken into account [3–5]. Variability [6] has also been introduced by employing a sigmoid function that allows reproducing the stochastic nature of the device physics. The model is suitable for implementation in circuit simulators to analyze circuits based on RRAMs under different operation regimes.

2. Fabricated devices

Two types of MIM devices have been fabricated: Pt/TiO_2/Al_2O_3/TiO_2/RuO_x/TiN and TiN/Ti/HfO_2/W.

The fabrication of RRAMs containing the TiO_2/Al_2O_3/TiO_2 stack was based on an ALD deposition performed in a flow-type reactor (substrate temperature of 350 °C). The Ti precursor was $TiCl_4$, the Al precursor was TMA and H_2O was used as oxygen source. $TiCl_4$ and TMA were kept at room temperature. In Fig. 1a and b the fabricated dielectric layer thicknesses and a schematic representation of the device cross-sections is shown.

The TiN/Ti/HfO_2/W structures were fabricated on (100) p-type CZ silicon wafers. Wet thermal oxidation was performed at 1100 °C to create a 200 nm thick SiO_2 layer. A deposition of a W layer (200 nm) by magnetron sputtering followed. After this process, an ALD deposited 10 nm thick HfO_2 was formed at 225 °C using H_2O and TDMAH as precursors. The top electrode consisted of a 200 nm TiN and a 10 nm Ti layer. Dry etching of the HfO_2 layer was employed for the bottom electrode contact windows. The device area was a 15 x 15μm^2 square. A schematic of the device cross-section is shown in Fig. 1c.

3. Model description

The model is based on the geometric scheme shown in Fig. 2a. The CF creation is linked to oxygen ion migration and the formation of percolation paths (the conductive filaments) made of oxygen vacancies [1–3,5]. The CF time evolution is described by the following equations

* Corresponding author.
E-mail address: jroldan@ugr.es (J.B. Roldán).

http://dx.doi.org/10.1016/j.mee.2017.04.019
0167-9317/

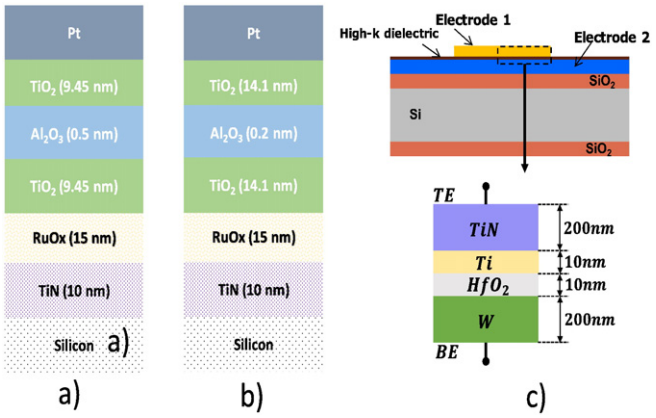

Fig. 1. Cross-section sketch of the fabricated devices based on the following stacks: a) $Pt/TiO_2(9.45\ nm)/Al_2O_3(0.5\ nm)/TiO_2(9.45\ nm)/RuO_x/TiN$, b) $Pt/TiO_2(14.1\ nm)/Al_2O_3(0.2\ nm)/TiO_2(14.1\ nm)/RuO_x/TiN$ and c) $TiN/Ti/HfO_2(10\ nm)/W$.

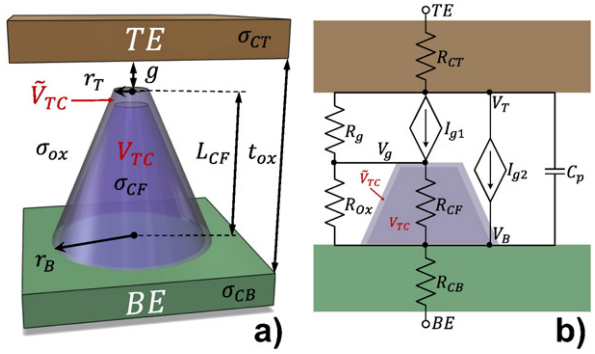

Fig. 2. a) RRAM geometrical scheme, CF features and main model variables. The variability has been implemented as a random volume variation ($V_{\sim TC}$), b) RRAM equivalent circuit including the different electrical components included in the model.

formulated in terms of the CF volume:

$$\frac{dV_{TC}}{dt} = v_0 \exp\left(-\frac{E_a - \alpha_a Z q \xi}{k_b T}\right) \text{ (set)} \tag{1}$$

$$\frac{dV_{TC}}{dt} = -v_0 \exp\left(-\frac{E_r - \alpha_r(g) Z q \xi}{k_b T}\right) \text{ (reset)} \tag{2}$$

V_{TC} stands for the CF volume, v_0 is obtained as the product of the oxygen vacancy volume and the oxygen atom vibration frequency [2], E_a is the oxygen vacancy activation energy, α_a is the electric field enhancement factor, Z is the oxygen ion charge number, q is the electron charge, ξ is the electric field, k_b is the Boltzmann constant, T stands for the local

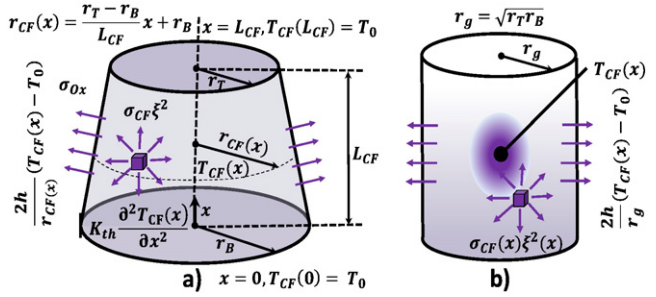

Fig. 3. a) Energy dissipation terms included in the heat equation, and geometrical domain for the CF thermal description, b) equivalent cylindrical CF employed to simplify the heat equation solution and to obtain a compact analytical expression for the CF temperature.

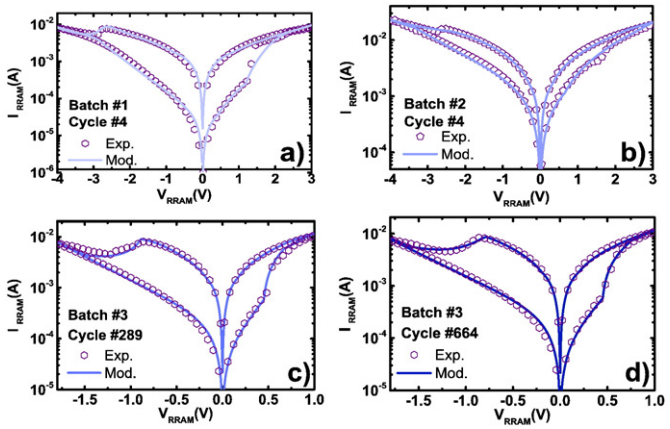

Fig. 4. Current versus voltage for different RS cycles of the samples under study: a) batch#1 cycle #4 b) batch#2 cycle #4 c) batch#3 cycle #289 and d) batch#3 cycle #664. The model reproduces accurately the experimental results.

temperature (obtained by solving the heat equation, see Fig. 3), E_r is an activation energy linked to the processes involved in the RESET process, and $\alpha_r(g)$ is a linear function of g that accounts for the electric field enhancement factor that induces a lowering of the hopping barrier and the external voltage enhancement factor during oxygen ions release [2].

The circuit that models the RRAM operation is sketched Fig. 2b. The scheme was used for the Verilog-A implementation of the model. The electrode ohmic resistances are R_{CT} and R_{CB}, the CF resistance is R_{CF}, the dielectric surrounding the CF resistance and the dielectric region filling the gap g associated resistance are R_{ox} and R_g, respectively. The nonlinear current sources that account for the hopping current are modeled through I_{g1} and I_{g2}. The latter depends on the CF geometry and on the voltage applied to the gap g. A capacitance (C_p) is also included [7].

The thermal characteristics are obtained by solving the heat equation within the CF [3,4,7],

$$\sigma_{CF}\xi^2 = -k_{th}\frac{\partial^2 T(x)}{\partial x^2} + 2h\frac{T(x) - T_{ox}}{r_{CF}(x)} \tag{3}$$

σ_{CF} stands for the CF electric conductivity (we assume metallic-like temperature dependence [3,7]), r_{CF} is the CF radius (variable because of a noncylindrical shape), ξ is the CF average electric field, k_{th} the CF thermal conductivity. The parameter h stands for heat transfer coefficient (accounts for the lateral heat dissipation from the CF to the dielectric). Eq. (3) cannot be solved analytically assuming a CF with variable r_{CF}. In order to obtain an approximated explicit solution we consider that a truncated-cone shaped CF with constant conductivity is

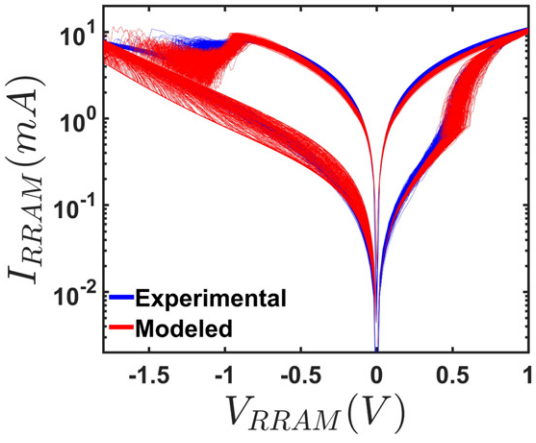

Fig. 5. a) Batch#3: 729 experimental cycles and 400 modeled cycles.

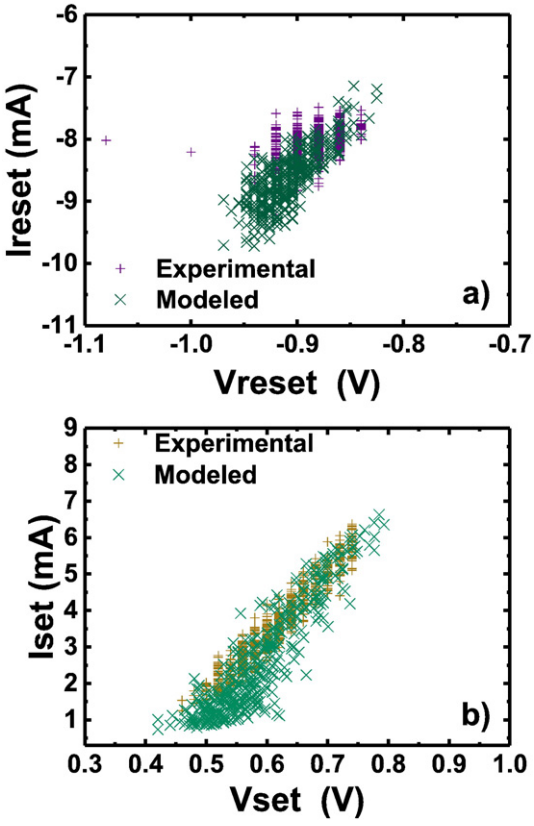

Fig. 6. Batch#3 a) I_{reset} versus V_{reset} calculated for experimental and simulated data. b) I_{set} versus V_{set} calculated for experimental and simulated data.

equivalent (after an algebraic transform) to a cylindrical CF with r_g radius (r_T (r_B) stands for the top (bottom) CF radius) and a conductivity dependent on the spatial variable along the CF main axis (see Fig. 3). With this asumption the cylinder maximum temperature found is given in Eq. (4) and it is assumed as the CF temperature,

$$T = T_0 + \frac{\sigma_{CF} r_g r_B \xi^2}{r_T h}\left[\frac{1}{2} - \frac{e^{\frac{\alpha}{2}}}{e^{\alpha}+1}\right] \tag{4}$$

where the α parameter is given below:

$$\alpha = L_{CF}\sqrt{\frac{2h}{k_{th} r_g}} \tag{5}$$

Finally, a random component $V_{\sim TC}$ is included as a variation of the CF volume to account for the device variability. In this manner V_{TC} can be obtained as follows:

$$V_{TC}(t) = \int \frac{dV_{TC}}{dt} dt + V_{\sim TC} \tag{6}$$

$$V_{\sim TC} = V_{TCrnd}(\Delta t) F(T) rnd \tag{7}$$

where V_{TCrnd} is a random number whose Gaussian distribution presents a null mean value and a standard deviation σ_{VTC}, *rnd* is a flag parameter to introduce variability in the model and $F(T)$ is a sigmoid function that depends on the temperature, since the CF volume variation is connected with the kinetic energy of ions [6] (see Eq. (8)):

$$F(T) = \frac{1}{2}\left[\tanh\left(\frac{T - T_c}{T_s}\right) + 1\right] \tag{8}$$

where T_C is a threshold temperature above which significant random variation of the gap size occurs, while T_S is a function smoothing parameter.

4. Results and discussion

The proposed model was tested for three different RRAM technologies (see Fig. 1). Batch#1 $Pt/TiO_2/Al_2O_3/TiO_2/Ru/Si$ with 19.4 nm oxide thickness (0.5 nm of Al_2O_3), batch#2 with the same structure than batch#1 and 28.4 nm oxide thickness (0.2 nm of Al_2O_3) and batch#3 $TiN/Ti/HfO_2/W$ with a dielectric 10 nm thick (see Figs. 4–5). The same physical constants were employed for all the I-V curves, the CF geometrical features were selected for each of the fitted curves in Fig. 4.

The variability is also correctly modeled as shown in Figs. 5 and 6 by using Eqs. (6) and (7). A better fit than in previous approaches [3] was obtained (see Fig. 6). The cumulative probabilities of R_{on}, R_{off} (Fig. 7 a) and of V_{set}, V_{reset} (Fig. 7 b) are also calculated, where a good agreement between the experimental and simulated data is observed.

The introduction of a threshold in a smooth sigmoid function makes sense since RS mechanisms, linked to cycle-to-cycle variability, are self-accelerated processes triggered by temperature. The good fit obtained in Figs. 6 and 7 shows that the selected approach is appropriate.

5. Conclusions

A physically based model for bipolar MIM resistive memories is presented including a detailed temperature and variability description. The model was tested for three different RRAM technologies and a good agreement was obtained between the experimental and simulated

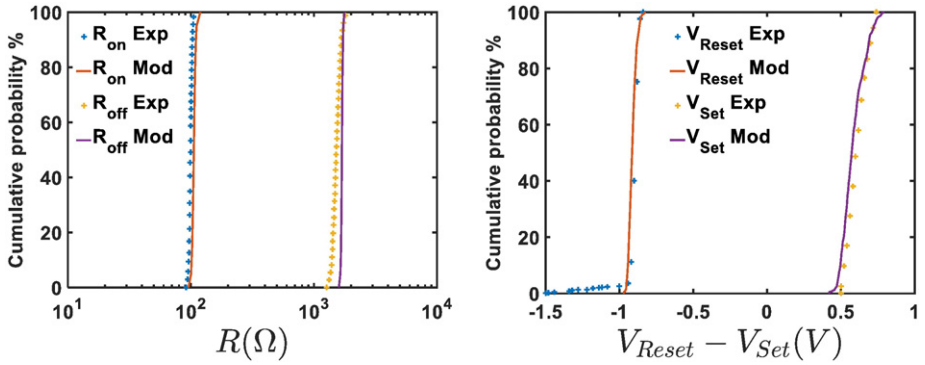

Fig. 7. Cumulative probability comparative between experimental and modeled data for batch#3: a) R_{on} and R_{off} @V = 0.1 V b) V_{reset} and V_{set}.

data. The thermal features and the variability were modeled reasonably well in all the cases considered.

Acknowledgements

This work was funded by the Spanish Ministry of Economy and Competitiveness and the FEDER Program through projects TEC2014-52152-C3-1-R, TEC2014-52152-C3-2-R, TEC2014-52152-C3-3-R and TEC2014-54906-JIN, and has made use of the Spanish ICTS Network MICRONANOFABS. Authors acknowledge Prof. Aarik group from the Institute of Physics (University of Tartu, Estonia) for providing some samples of this study.

References

[1] R. Waser, R. Dittmann, G. Staikov, K. Szot, Adv. Mater. 21 (2009) 2632–2663.
[2] P. Huang, et al., IEEE Trans. Electron Devices 60 (2013) 4090–4097.
[3] G. González-Cordero, F. Jiménez-Molinos, J.B. Roldan, M.B. González, F. Campabadal, J. Vac. Sci. Technol. B 35 (2017), 01A110. .
[4] M.A. Villena, M.B. González, J.B. Roldán, F. Campabadal, F. Jiménez-Molinos, F.M. Gómez-Campos, J. Suñé, Solid State Electron. 111 (2015) 47–51.
[5] G. González-Cordero, J.B. Roldán, F. Jiménez-Molinos, Conference on Design of Circuits and Integrated Systems (DCIS), 2016.
[6] X. Guan, S. Yu, H.S.P. Wong, IEEE Elec. Dev. Lett. 33 (2012) 1405–1407.
[7] G. González-Cordero, J.B. Roldán, F. Jiménez-Molinos, J. Suñé, S. Long, M. Liu, Semicond. Sci. Technol. 31 (2016) 115013.